Applied Catalysis B: Environmental 84 (2008) 100–105

Contents lists available at ScienceDirect

Applied Catalysis B: Environmental

journal homepage: www.elsevier.com/locate/apcatb

Hollow core/mesoporous shell carbon as a highly efficient catalyst support in direct formic acid fuel cell

Baizeng Fang, Minsik Kim, Jong-Sung Yu *

Department of Advanced Materials Chemistry, Korea University, 208 Seochang, Jochiwon, ChungNam 339-700, Republic of Korea

ARTICLE INFO

Article history:
Received 23 November 2007
Received in revised form 11 February 2008
Accepted 11 March 2008
Available online 20 March 2008

Keywords:
Hollow core/mesoporous shell carbon
Catalyst support
Anode
$Pt_{50}Ru_{50}$
Direct formic acid fuel cell

ABSTRACT

Spherical carbon capsules with a hollow macroporous core of ca. 260 nm and a ca. 40 nm thick mesoporous shell were explored for the first time as an anode catalyst support in direct formic acid fuel cell (DFAFC). Hollow core/mesoporous shell carbon (HCMSC) possesses fantastic structural characteristics such as uniform particle size, well-developed three-dimensionally interconnected bimodal porosity, and large specific surface area and pore volume, which are highly desired for a catalyst support in low temperature fuel cells. HCMSC-supported $Pt_{50}Ru_{50}$ (60 wt.%) has exhibited almost two times the power density that delivered by the commonly used catalyst support carbon black Vulcan XC-72 supported one, suggesting that the HCMSC is a highly efficient anode catalyst support in DFAFC.

1. Introduction

Direct fuel cells (DFCs) using liquid fuels directly as a fuel without a reforming step have received much attention in the past decade because liquid fuels are very easy to store, transport and refill, and allow for compact design that can offer up to 10 times the energy density of rechargeable batteries. In addition, DFCs can operate at ambient temperature, reducing thermal management challenges for small systems. These advantages make the technology attractive to the rapidly increasing need for portable power sources [1–7].

Direct formic acid fuel cell (DFAFC) has been attracting much interest recently because formic acid has many merits over methanol such as much lower crossover through a Nafion membrane [8], and safer and easier handling. In addition, electro-oxidation of formic acid on Pt-based catalyst is more efficient than that of methanol [9]. Hopefully, DFAFC will become one of the earliest commercialized small power sources among low temperature fuel cells [1]. However, compared with hydrogen-fed fuel cells, one of the main challenges that DFAFC has to face before its commercialization is the sluggish anode kinetics even on some state-of-the-art Pt-based anode catalysts. The slow anode kinetics stemming from a multi-step oxidation process of formic acid results in a high anodic polarization loss.

Two main approaches have been taken to improve the electro-oxidation of formic acid on Pt-based catalysts and meanwhile to lower the usage of Pt. One is alloying Pt with less expensive metals such as Pd [10,11], Ru [10–13], Bi [14,15], Pb [14], Sb [14,16], Ag [17], Se [18], Te [19], etc. To date, Ru has been proved one of the most widely investigated efficient promoters for Pt-based anode catalysts in DFAFC. The other is catalyst support technology, which has been proved a crucial factor in determining particle size and distribution of the supported catalyst nanoparticles, and accordingly has significant influences on catalytic performance and stability of the supported catalyst. An ideal support material should have the following characteristics: high inertness in harsh chemical and electrochemical conditions, large surface area for good dispersion of catalyst nanoparticles, well-developed porosity to allow efficient diffusion of reactants and products, high electrical conductivity, and low cost [20]. Carbon is the most promising candidate, which can satisfy most of such characteristics to be attractive as a catalyst support for fuel cells. It was found that the specific activity of supported Pt-Ru catalyst is much higher than unsupported Pt-Ru black in fuel cells. Reduction of the catalyst loading amount through increasing Pt utilization is one of the research avenues for catalyst cost reduction. Pt or Pt alloy supported on carbon black Vulcan XC-72 (VC) is widely used as an electro-catalyst in the DFAFC due to its relatively high catalytic activity and excellent chemical stability in the fuel cell environ-

* Corresponding author. Tel.: +82 41 860 1494; fax: +82 41 867 5396.
E-mail address: jsyu212@korea.ac.kr (J.-S. Yu).

0926-3373/$ – see front matter © 2008 Elsevier B.V. All rights reserved.
doi:10.1016/j.apcatb.2008.03.005

ment However, carbon black VC contains primary pores, which are too small to be filled by the electrolyte polymer, and many Pt-Ru nanoparticles trapped in the micropores of less than 1 nm of the carbon black were not involved in the electrochemical reactions on electrodes due to absence of the triple-phase boundaries (gas–electrolyte–electrode) [21].

Researches in direct methanol fuel cells (DMFC) have revealed that catalyst supports considerably affect catalytic activities of the supported Pt-based catalysts [22–27]. Nanostructured or nanoporous carbon materials, for instance, carbon nanotubes [28–31], graphitic carbon nanofibers [32,33], mesostructured carbon materials [26], carbon microbeads [34], macroporous carbons [35–37], hollow core mesoporous shell carbon capsule [38], periodically ordered bimodal porous carbon [25], and carbon nanocoils [39] have been reported to have better catalyst support effect than commercial carbon black VC for methanol oxidation.

Although it is also highly required to have highly efficient catalyst support for improving sluggish oxidation kinetics of formic acid, only VC has almost been exclusively investigated as a catalyst support in DFAFC. In this study, a novel anode catalyst support, hollow macroporous core/mesoporous shell carbon (HCMSC) has been explored for the first time to support $Pt_{50}Ru_{50}$ metal nanoparticles for DFAFC applications. HCMSC possesses an interconnected bimodal pore system, highly developed porosity and narrow pore size distribution. To our interest, twice the power density delivered by the VC-supported Pt-Ru catalyst has been demonstrated by the HCMSC-supported one.

2. Experimental

2.1. Synthesis of HCMSC

HCMSC was synthesized by using submicrometer-size solid core/mesoporous shell (SCMS) silica spheres as template [40]. SCMS was fabricated as follows: 40 mL of aqueous ammonia (32 wt.%) was added to a solution containing 1 L of ethanol and 80 mL of deionized water. After stirring at 30 °C for ca. 15 min, 60 mL of tetraethoxysilane (TEOS) was added to the above-prepared mixture and the reaction mixture was stirred for 6 h to yield uniform silica spheres. A mixture solution containing 50 mL of TEOS and 20 mL octadecyltrimethoxysilane (C_{18}-TMS) was added to the colloidal solution containing the silica spheres and further reacted for 1 h. The resulting octadecyl group incorporated silica shell/solid core nanocomposite was retrieved by centrifugation, dried at room temperature and further calcined at 823 K for 6 h under an oxygen atmosphere to produce the final SCMS silica material. Aluminum was incorporated into the silicate framework through an impregnation method. Typically, 1.0 g of SCMS silica was added to an aqueous solution containing 0.27 g of $AlCl_3{\cdot}6H_2O$ in 0.3 mL of water, and the resulting slurry was stirred for 30 min. The powder was dried in air at 353 K. Finally, the Al-impregnated SCMS silica was calcined at 823 K for 5 h in air to yield SCMS aluminosilicate.

A typical synthesis route for the HCMSC capsules is as follows. 0.374 g of phenol was incorporated into the mesopores of 1.0 g of SCMS template by heating at 100 °C for 12 h under static vacuum. The resulting phenol-incorporated SCMS template was reacted with paraformaldehyde (0.238 g) under static vacuum at 130 °C for 24 h to yield a phenol–resin/SCMS aluminosilicate composite. The composite was heated at 1 K/min to 160 °C and held for 5 h under a nitrogen flow. The temperature was then ramped at 5 K/min to 950 °C and held for 7 h to carbonize the cross-linked phenol resin inside the mesopores of the SCMS structure. The dissolution of the SCMS template using 2.0 N NaOH and washing in EtOH–H_2O solution (volume ratio of EtOH to H_2O = 1:1) produced the HCMSC.

2.2. Preparation of carbon-supported $Pt_{50}Ru_{50}$ catalysts and electrodes

Carbon-supported $Pt_{50}Ru_{50}$ (60 wt.%) alloy catalysts were prepared at room temperature through the impregnation method using $H_2PtCl_6{\cdot}6H_2O$ and $RuCl_3{\cdot}xH_2O$ as metal precursors and $NaBH_4$ as a reducing agent. Equal moles of Pt and Ru salts were dissolved in deionized water. The required amount of carbon was dispersed and stirred in deionized water to form homogeneous slurry. After addition of the metal salt solution into the carbon slurry, the mixture was adjusted to pH of 8 by addition of 3.0 M NaOH, followed by dropwise addition of excess $NaBH_4$ solution (molar ratio of $NaBH_4$ to the metal was about 10) under vigorous stirring. After being stirred overnight for complete reduction of Pt and Ru ions, the slurry was then filtered, rinsed with excess ethanol-water solution (in a volume ratio of 1:1) and deionized water, and dried at 70 °C overnight. 60 wt.% metal loading was made for carbon-supported catalysts, to compare fairly the HCMSC with the VC, and to compare the HCMSC-supported catalyst with the commercial E-TEK one (60 wt.% $Pt_{50}Ru_{50}$ loading). Metal loadings of the supported Pt-Ru catalysts on the HCMSC and VC were determined roughly as ca. 58 and 56 wt.%, respectively, by the thermogravimetric analysis (TGA).

For single cell tests, catalyst inks were prepared by dispersing various carbon-supported $Pt_{50}Ru_{50}$ nanoparticles (or unsupported Pt black, for the cathode catalyst layer) into an appropriate amount of mixture solution composed of deionized water and the required amount of 5 wt.% Nafion ionomer solution (Aldrich). The Nafion ionomer contents in the catalyst layers were set as 25 and 10 wt.% for the anode and cathode, respectively. Appropriate amount of the catalyst inks were painted uniformly on Teflonized carbon paper (TGPH-090) and dried at 70 °C overnight. The catalyst loadings were 3.0 mg/cm^2 (based on $Pt_{50}Ru_5$ alloy only) at the anode and 5.0 mg/cm^2 at the cathode (unsupported Pt from Johnson-Matthey). The MEA (membrane electrode assembly) was employed to construct a single fuel cell, which had been fabricated by hot-pressing a pretreated Nafion 117 (Du-Pont) membrane sandwiched by the anode and cathode layers.

Three-electrode electrochemical cell (i.e., half cell) was employed to estimate electrochemical active surface area and investigate the catalytic activity towards oxidation of formaic acid for various carbon-supported Pt-Ru catalysts. For estimation electrochemical active surface area, cyclic voltammetric (CV) measurements were conducted in 0.5 M H_2SO_4 at room temperature with a scan rate of 25 mV/s, and for examination of the catalytic activity towards oxidation of formaic acid, CV measurements were conducted in 1 M HCOOH–0.5 M H_2SO_4. In all cases, Pt gauze was used as a counter electrode and Ag/AgCl as a reference one. Electrolyte solution was deaerated by high-purity nitrogen for 1 h prior to any cyclic voltammetric measurement and stable voltammograms were recorded after 10 cycles. The working electrode was a thin layer of Nafion-impregnated catalyst cast on a glassy carbon disk (3 mm in diameter) embedded in a Teflon cylinder. The catalyst layer was obtained as follows: First, 5 mg of carbon-supported $Pt_{50}Ru_{50}$ (60 wt.%) catalyst was dispersed in 1 mL of solution of deionized water and ethanol (1:4 in volume ratio) and then mixed with 50 μL of Nafion solution (5 wt.% Nafion). Next, the mixture was sonicated for 1 h, and a quantity of 5 μL of slurry was pipetted and spread on the top of a glassy carbon disk. Finally, the catalyst-coated glassy carbon electrode was dried at 70 °C for 2 h to yield a loading of 0.1 mgPt/cm^2.

2.3. Surface characterization

N_2 adsorption and desorption isotherms were measured at 77 K on a KICT SPA-3000 Gas Adsorption Analyzer after the carbon was

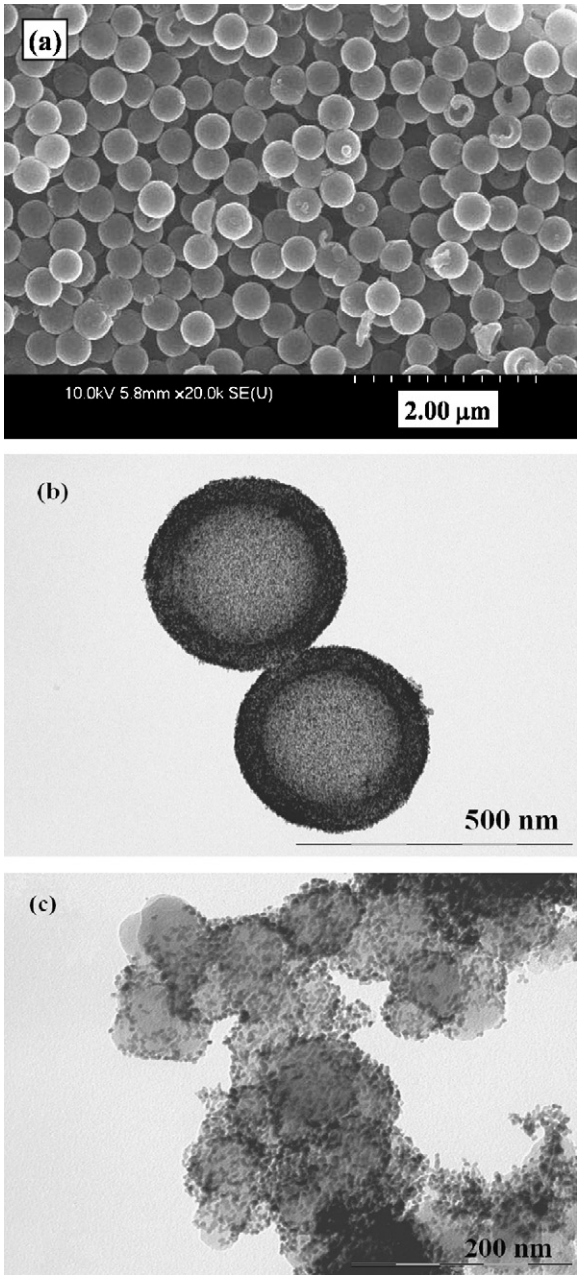

Fig. 1. SEM and TEM images for HCMSC (a), HCMSC-supported Pt-Ru catalyst (b) and VC-supported Pt-Ru catalyst (c). Black spots in (b) and (c) represent Pt-Ru nanoparticles.

degassed at 423 K to 20 μTorr for 12 h. The specific surface areas were determined from nitrogen adsorption using the Brunauer–Emmett–Teller (BET) equation. Total pore volume was determined from the amount of gas adsorbed at the relative pressure of 0.99. Micropore volumes of the porous carbons were calculated from the analysis of the adsorption isotherms using the Horvath–Kawzoe method. Pore size distribution (PSD) was derived from the analysis of the adsorption branch using the Barrett–Joyner–Halenda (BJH) method.

Scanning electron microscopy (SEM) images were obtained using a Hitachi S-4700 microscope operated at an acceleration voltage of 10 kV. The transmission electron microscopy (TEM) was operated on EM 912 Omega at 200 kV.

X-ray diffraction (XRD) measurements for carbon materials and supported $Pt_{50}Ru_{50}$ catalysts were carried out with a Rigaku 1200 using a Cu Kα radiation, a Ni β-filter and operating at 40 kV and 20 mA.

2.4. Fuel cell performance of carbon-supported $Pt_{50}Ru_{50}$ catalysts

Performance tests of fuel cells were conducted under constant current or constant voltage with a potentiometer (WMPG-1000). 3.0 M formic acid aqueous solution was supplied to the anode at a flow rate of 1.1 mL/min by a Masterflex liquid micro-pump, while dry O_2 was fed to the cathode at a rate of 200 mL/min through a flow meter.

3. Results and discussion

Fig. 1 shows representative SEM image for HCMSC (a) and TEM images for HCMSC- (b) and VC-supported $Pt_{50}Ru_{50}$ (60 wt.%) (c). The SEM image shows that the HCMSC capsules are produced as uniform individual discrete particles with diameter of ca. 340 nm. The TEM image of the HCMSC (not shown) reveals a core size of ca. 260 nm and shell thickness of ca. 40 nm. Fig. 1b shows that the Pt-Ru nanoparticles were dispersed homogenously as small, spherical and uniform dark spots over the entire surface of the HCMSC support. Pt-Ru nanoparticles supported on the HCMSC were measured to estimate a particle size of ca. 2–4 nm from the high resolution TEM image (not shown). The TEM image also shows that structural integrity of the HCMSC has been well preserved even after a high Pt-Ru loading of 60 wt.%. Randomly distributed mesopores of ca. 3 nm in the shell have been observed from the TEM image with high magnification (not shown), suggesting that the HCMSC capsules have a bimodal pore structure consisting of a spherical macroscopic core and a mesoporous shell. In contrast, Pt-Ru nanoparticles were dispersed unevenly on the VC surface with varying particles size as seen in Fig. 1c. Furthermore, large quantity of agglomeration of Pt-Ru nanoparticles was also observed somewhere from the VC-supported catalyst. Pt-Ru nanoparticles supported on the VC were found to have a wide particle size distribution of 1–5 nm from the high resolution TEM image (not shown).

Nitrogen adsorption–desorption isotherms for the HCMSC are shown in Fig. 2, which can be classified as a type IV isotherm with H_2-type hysteresis. The pore size from the PSD maximum was estimated as ca. 3.1 nm with a narrow PSD. The HCMSC exhibits a large specific surface area (ca. 1051 m^2/g) and total pore volume

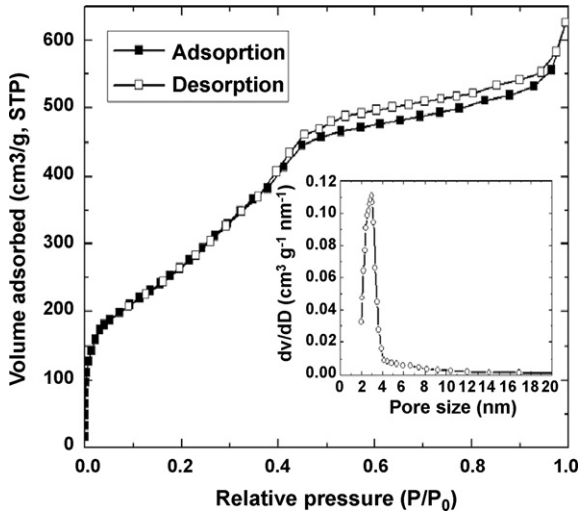

Fig. 2. Nitrogen adsorption–desorption isotherm at 77 K and derived PSD for the HCMSC.

Table 1
Surface structural parameters for the HCMSC and VC

Sample	S_{BET} (m^2/g)	V_{total} (cm^3/g)	V_{meso} (cm^3/g)	V_{micro} (cm^3/g)	Pore size (nm)
HCMSC	1051	1.26	0.91	0.35	3.1
VC	230	0.31	0.22	0.09	–

(ca. 1.26 cm^3/g), which are mainly attributable to the presence of the mesopores in the shell (mesopore volume: 0.91 cm^3/g). Structural parameters for the HCMSC and the VC derived from the N_2 adsorption–desorption isotherms are summarized in Table 1. It is clear that the HCMSC exhibits much larger BET surface area and mesoporous volume than the VC, implying that the HCMSC is a potential catalyst support for low temperature fuel cell applications.

Shown in Fig. 3 are typical XRD patterns for the HCMSC- and VC-supported Pt-Ru catalysts. All the XRD patterns exhibit the characteristic peaks of the Pt fcc structure. No peak was found related to tetragonal RuO_2 and hcp Ru phase, suggesting the presence of the Pt-Ru nanoparticles as an alloy. The average particle size of 2.7 nm was calculated for the HCMSC-supported $Pt_{50}Ru_{50}$ nanoparticles from the Pt (2 2 0) reflection of XRD patterns according to the Scherrer equation, which is smaller than that (4.3 nm) of the in-house VC-supported $Pt_{50}Ru_{50}$.

The TEM images and the XRD data suggest that it is feasible to synthesize a supported catalyst of high $Pt_{50}Ru_{50}$ loading with small Pt-Ru nanoparticle size together with a homogeneous dispersion of the nanoparticles if the support has large surface area, well-developed mesoporosity and a narrow PSD even though a simple impregnation route is taken for the synthesis of the catalyst.

Fig. 4a shows hydrogen electrosorption voltammetric profiles in 0.5 M H_2SO_4 for the HCMSC- and VC-supported Pt-Ru catalysts, from which electrochemical active surface area of the supported catalysts can be estimated through the integrated charge in the hydrogen absorption region of the steady-state cyclic voltammogram. Based on a monolayer hydrogen adsorption charge of 0.21 mC/cm^2 on Pt polycrystalline, and an assumption that Ru does not contribute to H adsorption, and after subtraction of the contribution of electrochemical double layer, the electrochemical active surface area was estimated to be 83 m^2/g for Pt in the HCMSC-supported Pt-Ru alloy nanoparticles catalyst, which is much higher than that (39 m^2/g) for Pt in $Pt_{50}Ru_{50}$ (60 wt.%)/VC. Higher electrochemical active surface area of the HCMSC-supported Pt-Ru catalyst results in part from the more uniform dispersion of Pt-Ru alloy nanoparticles with smaller particle size (average 2.7 nm) and narrower size distribution (i.e., 2–4 nm) on

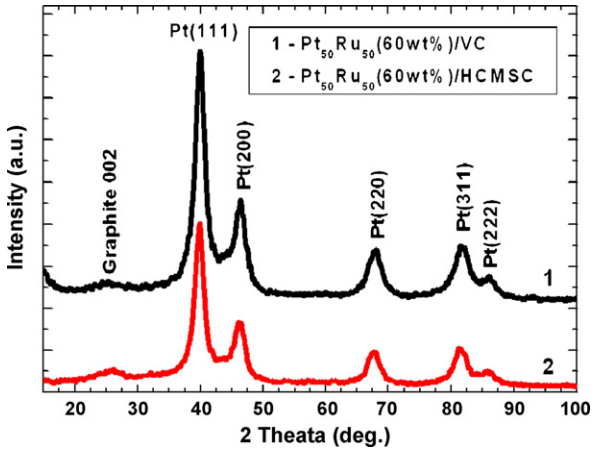

Fig. 3. Typical XRD patterns for the HCMSC- and VC-supported $Pt_{50}Ru_{50}$ catalysts.

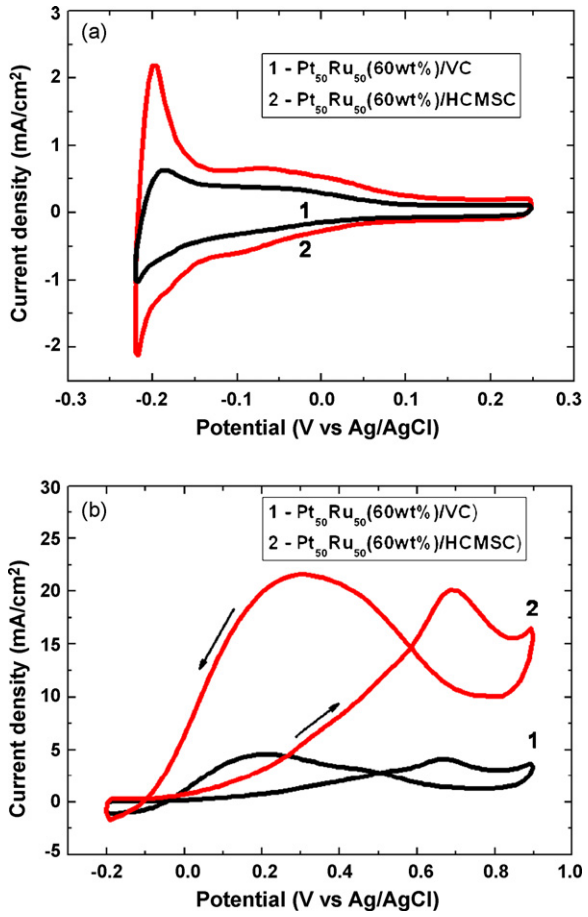

Fig. 4. Hydrogen electrosorption voltammetric profiles obtained in 0.5 M H_2SO_4 (a) and CV behaviour in 1 M HCOOH–0.5 M H_2SO_4 (b) for various carbon-supported Pt-Ru catalysts. Scan rate: 25 mV/s.

the HCMSC support than on the VC. In addition, the unique nanostructure of the HCMSC, namely, well-combined bimodal nanoporous structure with the mesopores in the shell open to outer surface and to the inner hollow macroporous core provides an open highway network around the active catalyst for efficient mass transport, also contributes to the high electrochemical active surface area. Higher electrochemical active surface area is supposed to provide the catalyst with higher catalytic activity. Fig. 4b shows CV behaviour in 1 M HCOOH–0.5 M H_2SO_4 for various carbon-supported Pt-Ru catalysts. A similar HCOOH oxidation behaviour to that reported by Wang et al. [8] for the Pt/C catalyst was observed. On the positive-going forward scan, two anodic peaks (wave) are observed. The first smaller anodic wave (starting at ca. 0.3 V) is contributable to the direct oxidation of HCOOH to CO_2 on the remaining sites unblocked by intermediate CO_{ads}, and the second larger anodic peak is contributable to the CO_{ads} oxidation, releasing the surface sites for the subsequent direct oxidation of HCOOH, as observed on the backward scan [8]. From Fig. 4b much higher electro-catalytic oxidation current of HCOOH is observed for the HCMSC-supported Pt-Ru catalyst than the VC-supported one. In addition, the HCMSC-supported Pt-Ru catalyst also shows a lower initiating potential for HCOOH oxidation, suggesting the HCMSC-supported Pt-Ru catalyst is more efficient than the VC-supported one for HCOOH oxidation.

Fig. 5 shows the cell polarization and power density plots for the various carbon-supported $Pt_{50}Ru_{50}$ (60 wt.%) anode catalysts at 30 °C (a) and 60 °C (b). At low current density (i.e., less than 25 mA/cm^2), fuel cell polarization is mainly under electrochemical

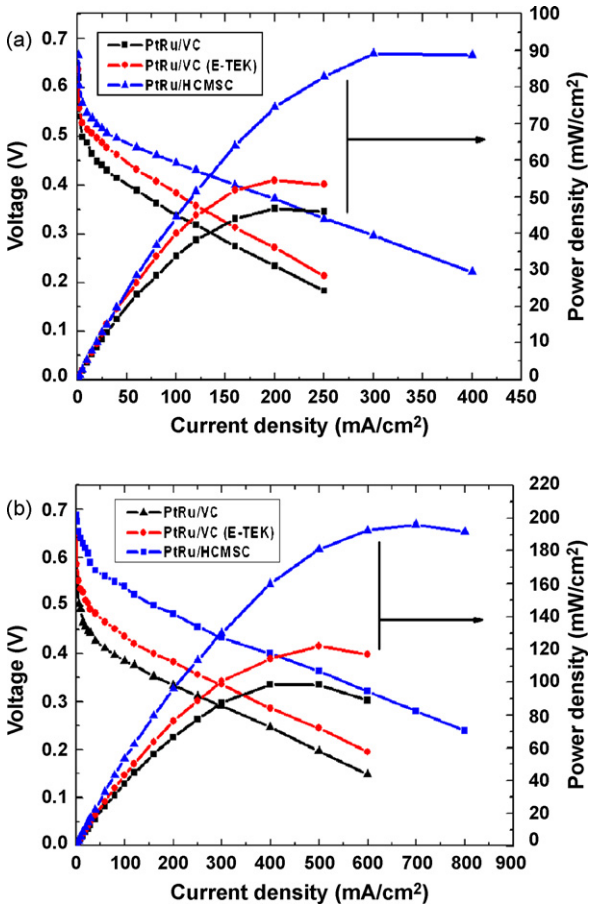

Fig. 5. Polarization and power density plots at 30 °C (a) and 60 °C (b) for various carbon-supported $Pt_{50}Ru_{50}$ (60 wt.%) anode catalysts.

activation control. In this region, appreciably smaller electrochemical polarization was observed from the HCMSC-supported anode catalyst than the VC-supported ones probably suggesting faster anodic oxidation kinetics on the surface of the former. The maximum power density for the HCMSC-supported $Pt_{50}Ru_{50}$ (60 wt.%) at 30 °C is ca. 89 mW/cm^2, which is 93% higher than the VC-supported one (ca. 46 mW/cm^2) and 65% higher than the E-TEK one (ca. 54 mW/cm^2). Similar improvement in the electrocatalytic activity towards the formic acid oxidation reaction and fuel cell performance were observed from the cell polarization plots obtained at 60 °C, where the HCMSC-supported $Pt_{50}Ru_{50}$ (60 wt.%) shows a maximum power density of ca. 196 mW/cm^2, which is almost twice that achieved by the VC-supported on (ca. 99 mW/cm^2), and 61% higher than the E-TEK one (ca. 122 mW/cm^2).

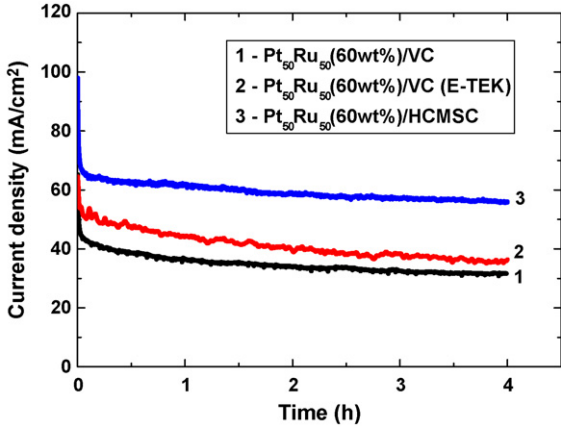

Fig. 6. Chronoamperograms obtained at 0.5 V and 30 °C for various carbon-supported $Pt_{50}Ru_{50}$ (60 wt.%) anode catalysts.

Fig. 6 shows chronoamperograms for the various carbon-supported $Pt_{50}Ru_{50}$ (60 wt.%) anode catalysts, which were obtained at 0.5 V and 30 °C. It was found that the HCMSC-supported $Pt_{50}Ru_{50}$ (60 wt.%) anode catalyst exhibits both higher initial and final current response within the tested time period, suggesting being significantly more active with respect to oxidation of formic acid compared to the VC-supported ones. At the end of test, the reaction current was ca. 56 mA/cm^2 for the $Pt_{50}Ru_{50}$/HCMSC, which is ca. 77% and 52% larger than that (ca. 31 mA/cm^2) for the $Pt_{50}Ru_{50}$/VC, and that (ca. 37 mA/cm^2) for the $Pt_{50}Ru_{50}$/VC (E-TEK), respectively. Such improvement in fuel cell polarization performance demonstrated by the HCMSC-supported Pt-Ru catalyst suggests that the HCMSC is a much more efficient anode catalyst support than VC for DFAFC application.

The considerable improvement in the electro-catalytic activity and fuel cell performance is attributable to the supporting effect of the HCMSC, related to its unique structural properties. Larger specific surface area and pore volume of the HCMSC favor a better dispersion of the supported catalyst together with smaller nanoparticle size, resulting in more active reaction sites for the oxidation of formic acid as evident from the TEM images, XRD patterns and electrochemical active surface area measurement. Spheres with short mesopore channels are also beneficial for applications limited by intraparticle diffusion processes such as catalysis and guest molecule encapsulation, enabling fast mass transfer through. The HCMSC has a thin mesopore shell of ~40 nm in thickness good for catalyst loading and efficient diffusion, which provides advantages over conventional ordered mesoporous carbon, which usually has long mesopore channels in a wide range of length scale of several hundred nanometers to several tens of micrometers even with bent morphologies depending upon the synthesis conditions [26]. In addition, the well-combined bimodal nanoporous structure with the mesopores in the shell open to outer surface and to the inner hollow macroporous core provides an open highway network around the active catalyst for efficient mass transport. Furthermore, the three-dimensionally interconnected large interstitial spaces between the packed spherical carbon particles, unique in this system, are open to the mesoporous channels, serving as primary fast pathways for the delivery of the reactants and products. In contrast, randomly distributed pores with varying size in the VC may result in less efficient mass transport.

4. Conclusions

HCMSC capsules with a hollow core of ca. 260 nm and a shell thickness of ca. 40 nm were synthesized and explored for the first time as the anode catalyst support in DFAFC. The superb structural characteristics such as larger surface area and pore volume, uniform particle size, well-developed three-dimensionally interconnected bimodal porosity enable the HCMSC to be an ideal catalyst support for low temperature fuel cell. The HCMSC-supported $Pt_{50}Ru_{50}$ (60 wt.%) catalyst exhibits higher catalytic activity towards the formic acid oxidation and much better fuel cell performance than the commercial carbon black VC-supported ones. The core size, shell thickness, porosity and surface morphology of the HCMSC capsules can be tailored by monitoring the size of the silica sphere, the amount and ratio of TEOS and C_{18}-TMS added, type of carbon precursors, surface activation and thermal treatment. This work is under investigation.

Acknowledgements

Authors would like to thank the KICOS for financial support toward Korea-Italy Joint Project, BK21 Program, and the Korean Basic Science Institute at Jeonju and Daejeon for SEM, TEM and XRD measurements.

References

[1] W.-M. Qian, David P. Wilkinson, J. She, H.-J. Wang, J.-J. Zhang, J. Power Sources 154 (2006) 202–213.
[2] B.D. Bath, H.S. White, E.R. Scott, Anal. Chem. 72 (2000) 433–442.
[3] C. Rice, S. Ha, R.I. Masel, P. Waszczuk, A. Wieckowski, T. Barnard, J. Power Sources 111 (2002) 83–89.
[4] P. Waszczuk, T.M. Barnard, C. Rice, R.I. Masel, A. Wieckowski, Electrochem. Commun. 4 (2002) 599–603.
[5] S. Ha, C. Rice, R.I. Masel, A. Wieckowski, J. Power Sources 112 (2003) 655–659.
[6] Y. Rhee, S. Ha, R.I. Masel, J. Power Sources 117 (2003) 35–38.
[7] C.R. Emerilis, Z. Gál, A.C.D. Angelo, C. Lind, F.J. DiSalvo, H.D. Abruña, ChemPhysChem 4 (2003) 193–199.
[8] X. Wang, J.-M. Hu, I.-M. Hsing, J. Electroanal. Chem. 562 (2004) 73–80.
[9] J. Willsau, J. Heitbaum, Electrochim. Acta 31 (1986) 943–948.
[10] C. Rice, S. Ha, R.I. Masel, A. Wieckowski, J. Power Sources 115 (2003) 229–235.
[11] G.Q. Lu, A. Crown, A. Wieckowski, J. Phys. Chem. B 103 (1999) 9700–9711.
[12] H.A. Gasteiger, N. Markovic, Philip N. Ross Jr, E.J. Cairns, Electrochim. Acta 39 (1994) 1825–1832.
[13] Y.Y. Tong, H.S. Kim, P.K. Babu, P. Waszczuk, A. Wieckowski, E. Oldfield, J. Am. Chem. Soc. 124 (2002) 468–473.
[14] M. Watanabe, M. Horiuchi, S. Motoo, J. Electroanal. Chem. Interfacial Electrochem. 250 (1988) 117–125.
[15] S.J. Kang, J.Y. Lee, J.K. Lee, S.-Y. Chung, Y.S. Tak, J. Phys. Chem. B 110 (2006) 7270–7274.
[16] Y.Y. Yang, S.G. Sun, Y.J. Gu, Z.Y. Zhou, C.H. Zhen, Electrochim. Acta 46 (2001) 4339–4348.
[17] A.H. Taylor, S. Kirkland, S.B. Brummer, Trans. Faraday Soc. 67 (1971) 819–827.
[18] M.J. Llorca, E. Herrero, J.M. Feliu, A. Aldaz, J. Electroanal. Chem. 373 (1994) 217–225.
[19] E. Herrero, M.J. Llorca, J.M. Feliu, A. Aldaz, J. Electroanal. Chem. 383 (1995) 145–154.
[20] K.-Y. Chan, J. Ding, J.-W. Ren, S.-A. Cheng, K.-Y. Tsang, J. Mater. Chem. 14 (2004) 505–516.
[21] D.R. Rolison, Science 299 (2003) 1698–1701.
[22] M. Watanabe, H. Sei, P. Stonehart, J. Electroanal. Chem. 261 (1989) 375–387.
[23] J.-S. Yu, S. Kang, S.B. Yoon, G. Chai, J. Am. Chem. Soc. 124 (2002) 9382–9383.
[24] A.S. Arico, S. Srinivasan, V. Antonucci, Fuel Cells 2 (2001) 133–136.
[25] G.S. Chai, I.S. Shin, J.-S. Yu, Adv. Mater. 16 (2004) 2057–2061.
[26] G.S. Chai, S.B. Yoon, J.-S. Yu, Carbon 43 (2005) 3028–3031.
[27] K. Lee, J. Zhang, H. Wang, D.P. Wilkinson, J. Appl. Electrochem. 36 (2006) 507–522.
[28] W. Li, C. Liang, W. Zhou, J. Qiu, Z. Zhou, G. Sun, Q. Xin, J. Phys. Chem. B 107 (2003) 6292–6299.
[29] C. Wang, M. Waje, X. Wang, J.M. Tang, R.C. Haddon, Y. Yan, Nano Lett. 4 (2004) 345–348.
[30] W. Li, X. Wang, Z. Chen, W. Waje, Y. Yan, Langmuir 21 (2005) 9386–9389.
[31] Z.Q. Tian, S.P. Jiang, Y.M. Liang, P.K. Shen, J. Phys. Chem. B 110 (2006) 5343–5350.
[32] C.A. Bessel, K. Laubernds, N.M. Rodriguez, R.T. Baker, J. Phys. Chem. B 105 (2001) 1115–1118.
[33] E.S. Steigerwalt, G.A. Deluga, D.E. Cliffel, C.M. Lukehart, J. Phys. Chem. B 105 (2001) 8097–8101.
[34] Y.C. Liu, X.P. Qiu, Y.Q. Huang, W.T. Zhu, G.S. Wu, J. Appl. Electrochem. 32 (2002) 1279–1285.
[35] G.S. Chai, S.B. Yoon, J.-S. Yu, J.-H. Choi, Y.-E. Sung, J. Phys. Chem. B 108 (2004) 7074–7079.
[36] F. Su, X.S. Zhao, Y. Wang, J. Zeng, Z. Zhou, J.Y. Lee, J. Phys. Chem. B 109 (2005) 20200–20206.
[37] M. Kim, S. Hwang, J.-S. Yu, J. Mater. Chem. 17 (2007) 1656–1659.
[38] G.S. Chai, S.-B. Yoon, J.-H. Kim, J.-S. Yu, Chem. Commun. (2004) 2766–2767.
[39] T. Hyeon, S. Han, Y.-E. Sung, K.-W. Park, Y.-W. Kim, Angew. Chem. Int. Ed. 42 (2003) 4352–4356.
[40] S.-B. Yoon, K. Sohn, J.-Y. Kim, C.-H. Shin, J.-S. Yu, T. Hyeon, Adv. Mater. 14 (2002) 19–21.